SUPPLEMENTARY MATERIAL

Supplementary figure 1

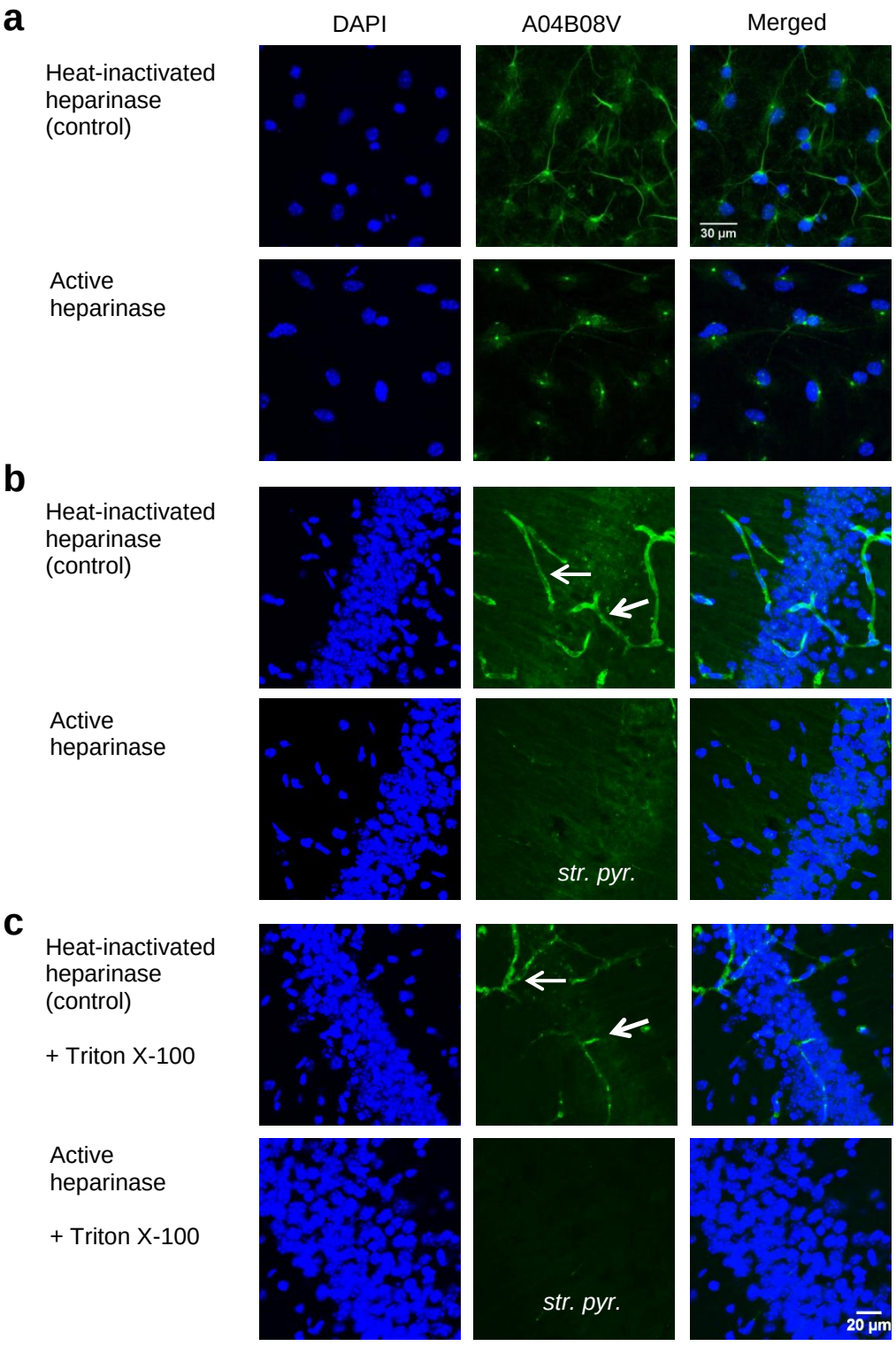

Analysis of heparinase 1 treatment efficacy. Dissociated hippocampal cultures (**a**, 24 days in vitro) and acute hippocampal slices (**b**, **c**) were incubated with active heparinase or heat-

inactivated heparinase (control treatment) and labeled with the anti-HS antibody A04B08V (Dam *et al.*, 2003; Kurup *et al.*, 2007) as described in Material and Methods.

a) Reduction of heparan sulfate (HS) membrane staining in dissociated cultures.

b) Complete loss of blood vessel HS staining (arrows) reveal digestion of HSs by heparinase 1 treatment.

c) Permeabilization with Triton-X 100 gives heparinase access to intracellular HSs. Note almost complete absence of HSs labelling including blood vessels after heparinase 1 treatment (*str. pyr.*, *stratum pyramidale*).

Supplementary figure 2

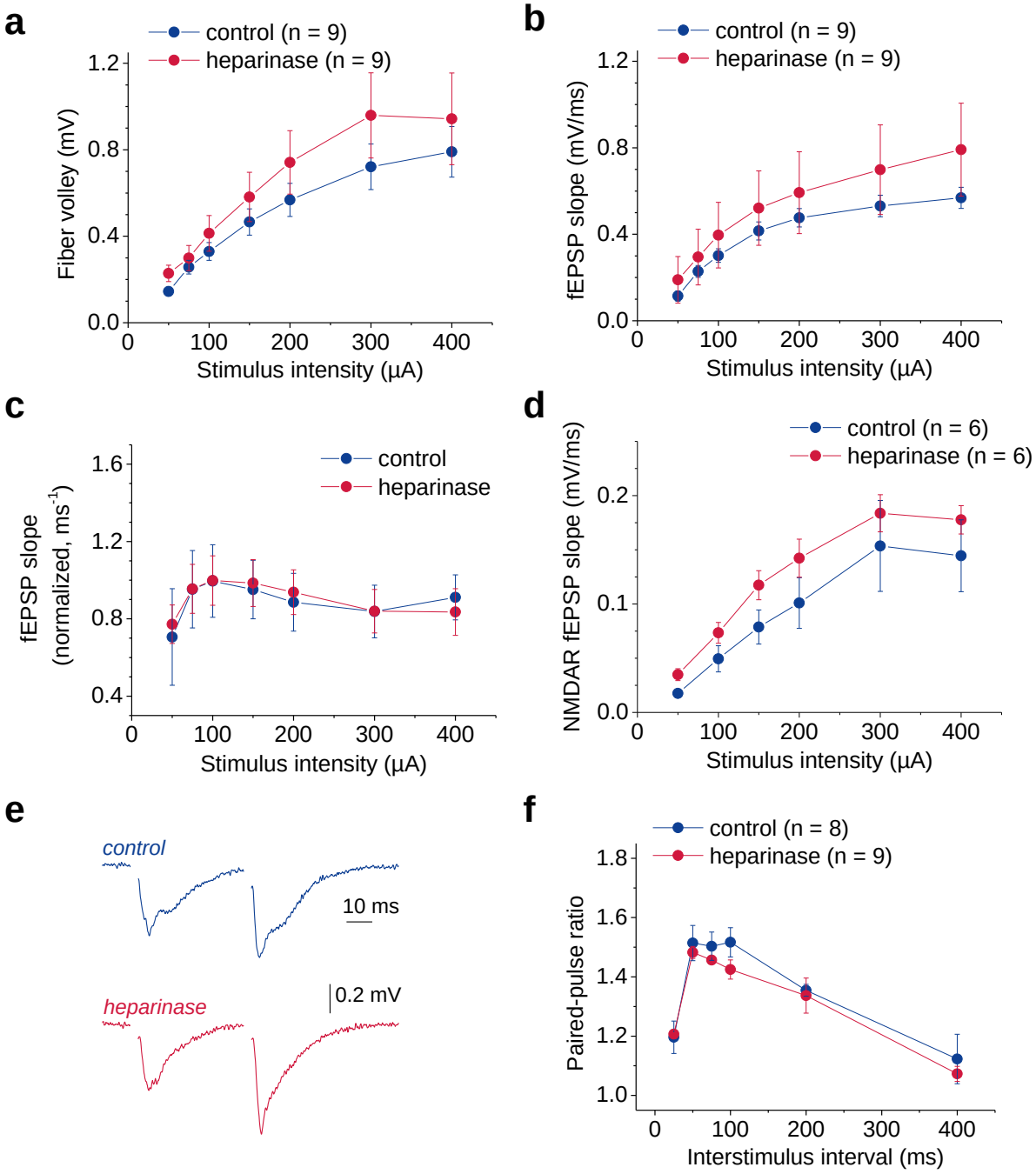

Heparinase treatment does not affect excitatory synaptic transmission at Schaffer collaterals. Field EPSPs (fEPSPs) were recorded from the *stratum radiatum* of the CA1 region. Axonal fiber volleys and fEPSP in response to single and paired stimuli were recorded from heparinase and control slices and analysed.

a) The amplitude of the axonal fiber volley was used as a measure of axonal excitability. No significant effect of heparinase treatment was detected (two-way repeated measures ANOVA $p = 0.30$).

b) fEPSP slopes did not differ between control and heparinase treated slices (two-way repeated measures ANOVA $p = 0.31$) indicating that postsynaptic responses were not affected by removal of heparan sulfates.

c) To account for variable activation of axons between experiments, fEPSP slopes were normalized to the average fiber volley amplitudes in each experiment. Normalized fEPSP slopes were virtually indistinguishable between control and heparinase treated slices (two-way repeated measures ANOVA $p = 0.92$ throughout, data for 100 µA stimulus intensity same as in figure 1).

d) NMDAR-mediated fEPSPs were pharmacologically isolated by recording in the presence of reduced extracellular Mg^{2+} (0.1 mM) and the AMPA receptor inhibitor NBQX (see also Methods). NMDAR-mediated fEPSP slopes did not differ between control and heparinase treated slices (n = 6 both groups, two-way repeated measures ANOVA $p = 0.23$, data for 100 µA stimulus intensity same as in figure 1).

e-f) The paired-pulse ratio (PPR) of fEPSP slope was used as indirect indicator of presynaptic release probability. Heparinase treatment did not significantly change the PPR compared to control treated slices (two-way repeated measures ANOVA $p = 0.28$, 50 ms data same as in figure 1).

Supplementary figure 3

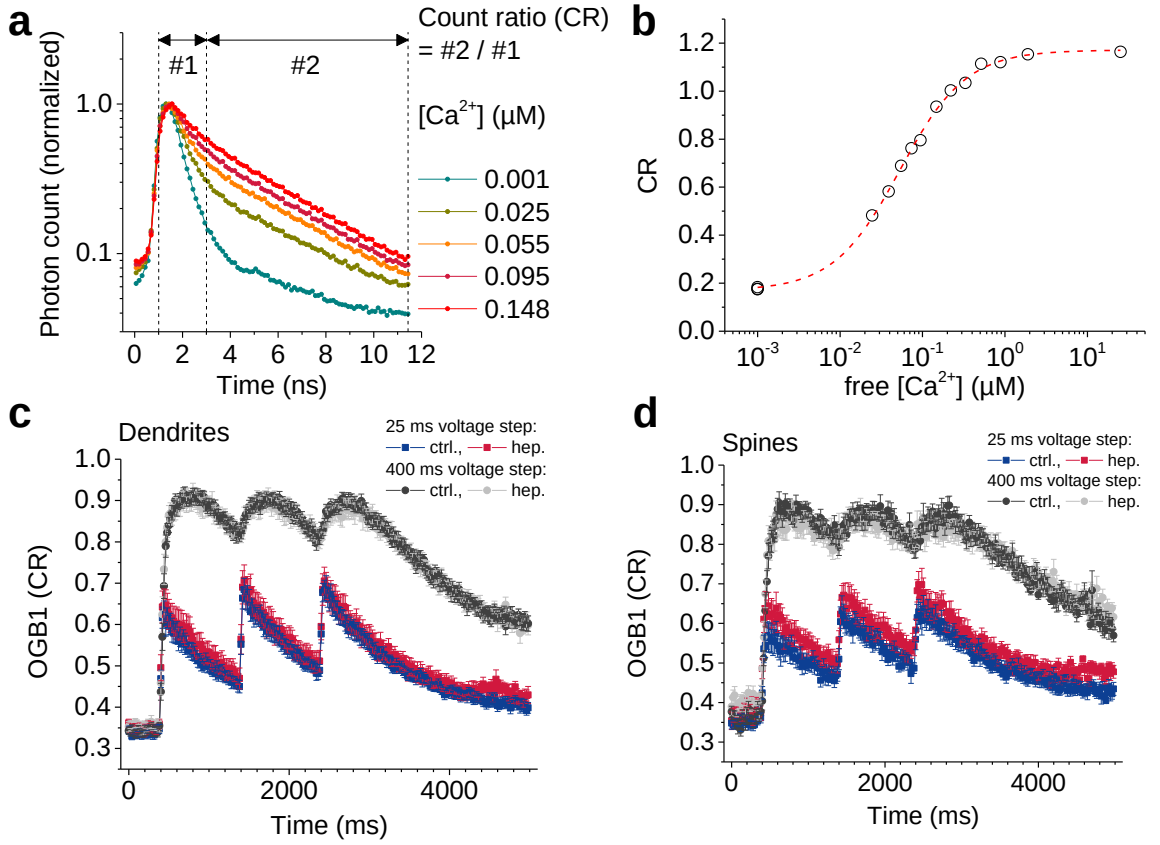

Fluorescence lifetime imaging (FLIM) of Oregon Green 488 BAPTA-1 (OGB1) in spines and dendrites of control/heparinase treated CA1 pyramidal cells. The fluorescence lifetime of the Ca^{2+} indicator OGB1 is known to depend on Ca^{2+} binding (Agronskaia *et al.*, 2004; Zheng *et al.*, 2015).

a) Lifetime profiles of OGB1 were obtained by time-correlated single photon counting in the presence of different [Ca^{2+}] and normalized to the peak photon count. Note the emerging slow lifetime component as [Ca^{2+}] increases. Lifetimes were quantified by calculating the photon count ratio (CR) by normalizing the photon count in time bin #2 to the photon count in bin #1.

b) CR is sensitive to changes [Ca^{2+}] and the relationship can be fitted by the sigmoid function $(A_1 - A_2) / (1 + [Ca^{2+}] / x_0)^P) + A_2$ with $A_1 = 0.169$, $A_2 = 1.171$, $x_0 = 0.053$ and $p = 1.08$ ($R^2 = 0.9987$, $p < 0.0001$).

c-d) FLIM of OGB1 was performed in CA1 pyramidal cell spines and dendrites in the presence of the sodium channel inhibitor TTX (1 µM), NBQX (10 µM), AP5 (50 µM), picrotoxin (100 µM), CGP52432 (5 µM), (K^+ based intracellular solution, n = 10 - 12). CA1 pyramidal cells were loaded via the whole-cell patch pipette with OGB1 (200 µM) and Alexa Fluor 594 (20 µM, see also figures 2 and 3 for an illustration). Line scans were performed across dendritic segments and spines and Ca^{2+} influx was evoked by three 25 ms (lower traces) and 400 ms (upper traces) voltage steps from a holding potential of -70 mV to +20 mV. CR values for 400 ms long depolarizations plateau well above peak values for 25 ms long depolarization. This indicates that the latter are not affected by dye saturation. Please see figure 3 for Ca^{2+} concentrations and statistics.

Supplementary figure 4

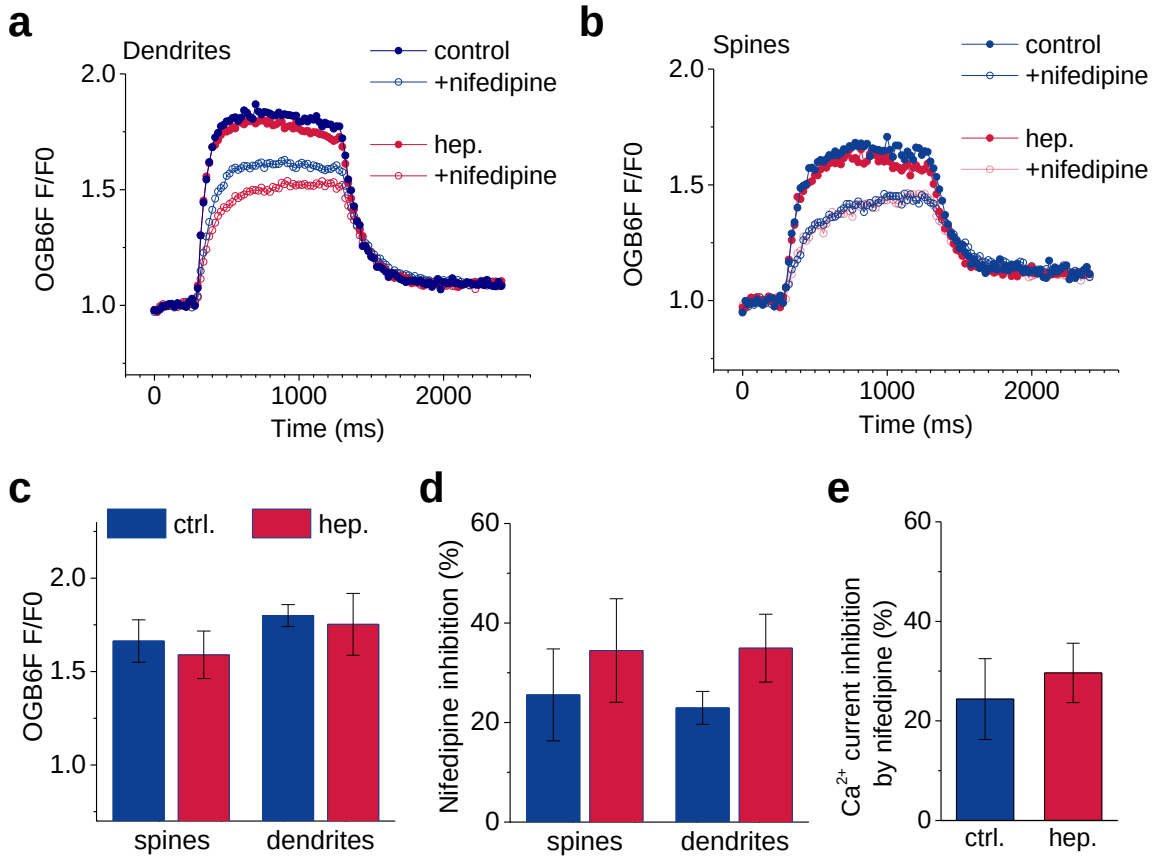

Heparinase treatment does not impair Ca^{2+} entry through L-type voltage gated Ca^{2+} channels (VGCC) in CA1 pyramidal cells.

a-b) CA1 pyramidal cells were filled with the low affinity Ca^{2+} indicator Oregon Green 488 BAPTA-6F (OGB6F, 250 µM) as illustrated in figure 2 and 3. To improve voltage control a Cs^{+}-based intracellular solution was used and the bath solution was supplemented with TTX 1 µM, NBQX 10 µM, AP5 50 µM, picrotoxin 100 µM and CGP52432 5 µM). The extracellular Ca^{2+} concentration was lowered to 0.35 mM (Mg^{2+} 2.95 mM) to limit Ca^{2+} entry to the dynamic range of OGB6F. Ca^{2+} entry through voltage gated Ca^{2+} channels was evoked by a one second voltage step from a holding potential of -50 mV to +20 mV. OGB6F fluorescence changes before (filled circles) and after (open circles) application of the L-type Ca^{2+} channel blocker nifedipine (20 µM) in control (blue) and heparinase-treated (hep., red) are shown (global averages, error bars omitted for clarity).

c) Total Ca^{2+} entry was quantified in spines and dendrites at 1000 ms and no significant differences were detected between control and heparinase treated slices (spines: control 1.59 ± 0.13, n = 9, heparinase 1.66 ± 0.11, n = 10, p = 0.67; dendrites: control 1.80 ± 0.06, n = 10, heparinase 1.75 ± 0.17, n = 10, p = 0.79, unpaired Student's t-tests). The slope of F/F0 over the initial 40 ms was used as a measure of local Ca^{2+} current and did not differ between control and heparinase treated slices (p = 0.65 and 0.97 for spines and dendrites, respectively, unpaired Student's t-tests).

d) The contribution of L-type VGCCs to Ca^{2+} influx was determined by calculating the percentage of ΔF/F0 reduction by nifedipine. No significant difference was detected (spines: control 25.6 ± 9.2, n = 9, heparinase 34.5 ± 10.4 %, n = 10, p = 0.53; dendrites: control 22.9 ± 3.3 %, n = 10, heparinase 35.0 ± 6.9 %, n = 10, p = 0.14, unpaired Student's t-tests).

e) Somatic Ca^{2+} currents of CA1 pyramidal cells were recorded as described previously (Kochlamazashvili *et al.*, 2010). Their inhibition by the L-type VGCC blocker nifedipine was similar to imaging experiments and not different between control and heparinase treated slices (control 24.4 ± 8.1 %, n = 4, heparinase 29.6 ± 6.0 %, n = 5, p = 0.62; unpaired Student's t-tests).

Supplementary figure 5

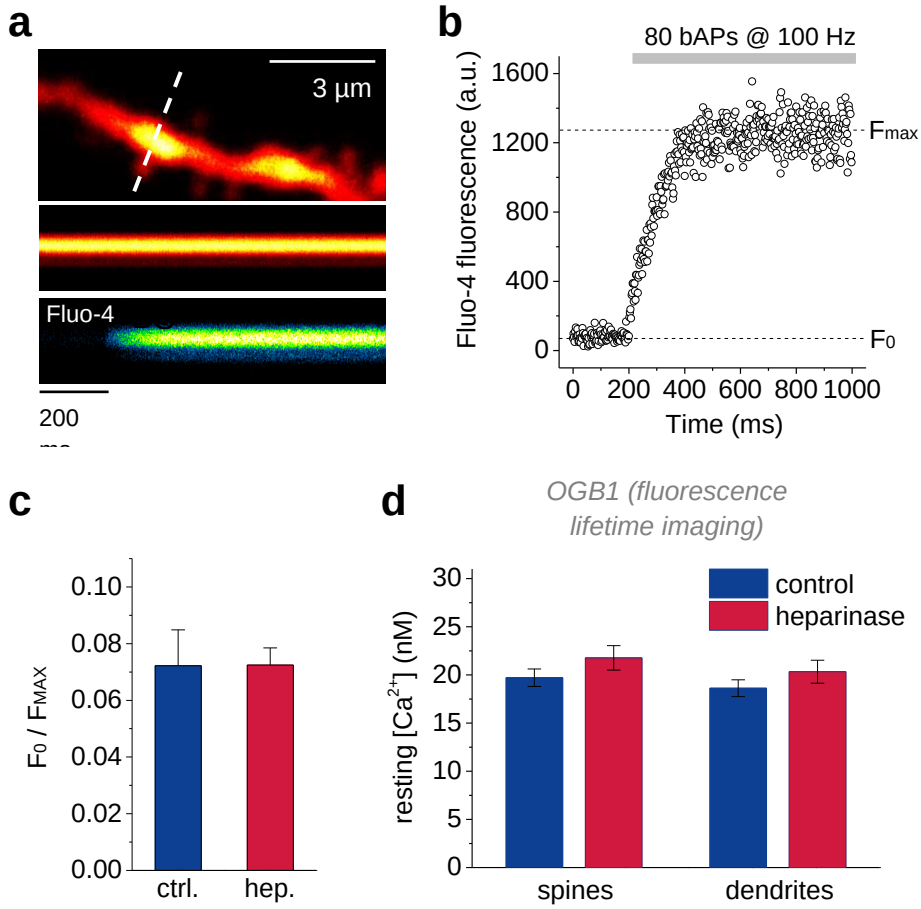

Heparinase treatment does not affect dendrite or spine resting Ca^{2+} concentrations. Two imaging approaches were used.

a-b) CA1 pyramidal cells were held in the whole-cell patch-clamp configuration in voltage clamp and filled with Alexa Fluor 594 and the Ca^{2+} indicator Fluo-4. Line scans were performed on pseudo-randomly chosen dendritic segments as illustrated. After a baseline period back-propagating action potentials (bAPs) were induced to saturate the Ca^{2+} indicator (Ermolyuk *et al.*, 2012). The resting Ca^{2+} concentration was then estimated by calculating the ratio F_0 / F_{MAX}.

c) No significant differences between CA1 pyramidal cells in control and heparinase treated slices were detected (n = 4 and 8 cells, p = 0.63, two-population Student's t-test).

d) Fluorescence lifetime imaging of CA1 pyramidal cells filled with OGB1 via the patch pipette was used as an alternative measure of resting [Ca^{2+}]. The average resting Ca^{2+} concentration was determined at spines and dendrites of CA1 pyramidal cells in control and heparinase treated hippocampal slices using OGB1 (n = 11, 9, 13 and 13 cells from left to right). No significant differences were detected in spines or dendrites (p = 0.21 and 0.26, two populations Student's t-test).

Supplementary figure 6

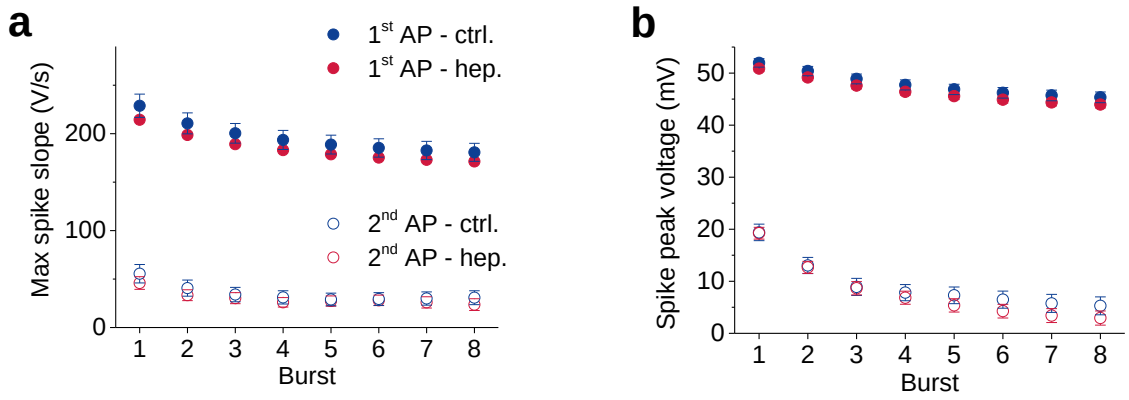

Action potential properties during TBS-like current injections. The maximum depolarization rate and the peak spike voltage were used to estimate Na^+ channel availability in control and heparinase treated slices.

a) A small (< 10% on average) reduction of the maximum depolarization rate of spikes was observed in heparinase treated slices (two-way repeated measures ANOVAs p = 0.482 and 0.409 for 1st and 2nd spike, n = 13 for both control [blue] and heparinase [red]; filled circles, 1st spike, empty circles 2nd spike).

b) No significant effect of heparinase treatment on the peak spike voltage was observed (two-way repeated-measures ANOVAs p = 0.631 and 0.575 for 1st and 2nd spike, same colour coding as in **a**). Also, no significant differences between spike half-widths were observed (two-way repeated-measures ANOVAs p = 0.685 and 0.353 for 1st and 2nd spike).

Supplementary figure 7

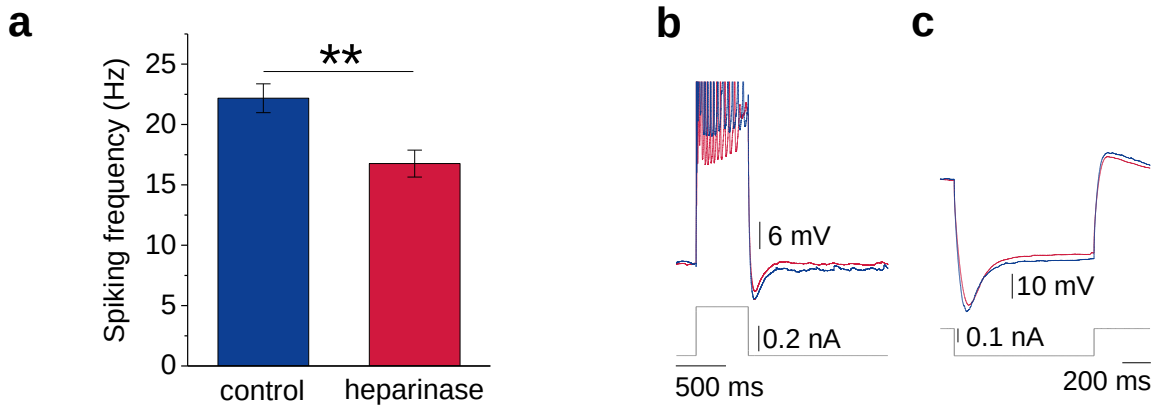

d

	control	heparinase	t-test
Resting membrane potential (mV)	-66.0 ± 1.2 (13)	-65.4 ± 1.1 (12)	*p* = 0.716
R_{in} (MΩ)	279.3 ± 29.1 (13)	248.4 ± 25.3 (12)	*p* = 0.838
Current threshold for spike within 300 ms (pA)	65.8 ± 7.9 (24)	74.0 ± 7.1 (20)	*p* = 0.446
Current threshold for spike within 40 ms (pA)	123.4 ± 13.4 (24)	142.3 ± 12.4 (20)	*p* = 0.306
Access resistance (MΩ)	13.5 ± 0.7 (24)	14.3 ± 1.0 (20)	*p* = 0.838
Voltage sag (mV)	23.3 ± 2.4 (13)	20.8 ± 1.2 (12)	*p* = 0.372
AHP amplitude (mV)	7.7 ± 0.5 (13)	7.2 ± 0.6 (12)	*p* = 0.485

Electrophysiological properties of CA1 pyramidal cells in control and heparinase treated slices.

a) Average spiking frequency during a 1000 ms long current injection (twice the current needed to evoke a single spike). Holding current was set to adjust the resting membrane potential to -70 mV (n = 19 for control and 17 for heparinase treatment, unpaired t-test, *p* = 0.0022).

b-c) Sample traces and protocols for recording the medium afterhyperpolarization (AHP) and I_H-dependent sag potentials.

d) Summary statistics of **b-c** and additional properties of CA1 pyramidal cells in control and heparinase treated slices.

Supplementary figure 8

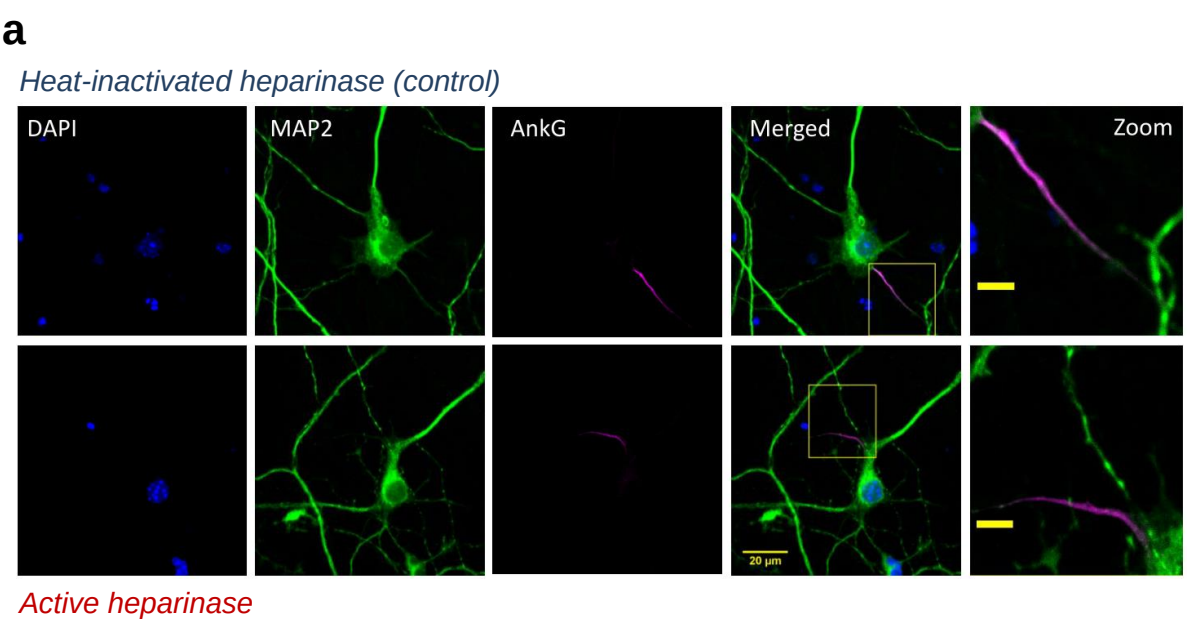

Ankyrin G (AnkG) is reduced in the distal axon initial segment after heparinase treatment.

a) Dissociated hippocampal cultures (DIV 21) prepared from mice were immunostained with Ankyrin G (AnkG) antiserum (magenta) and MAP2 (green). Scale bar for zoomed image is 5 µm.

b) The axonal AnkG distribution was determined by taking a 40 µm long fluorescence intensity line profile along the AnkG-immunofluorescence starting from the edge of the soma (identified using MAP2 immunofluorescence). Intensity profiles were obtained from four coverslips for each group (control/heparinase). A total of 23 (control) and 20 (heparinase) profiles were analysed. The average AnkG immunofluorescence values per 5 µm were used for two-way repeated measures ANOVA on ranks (treatment, $p = 0.032$). AnkG immunofluorescence was significantly reduced after heparinase treatment specifically at the distal part of axon initial segment (15-30 um, * $p < 0.05$, ** $p < 0.01$, Holm-Sidak post-hoc test).

Supplementary figure 9

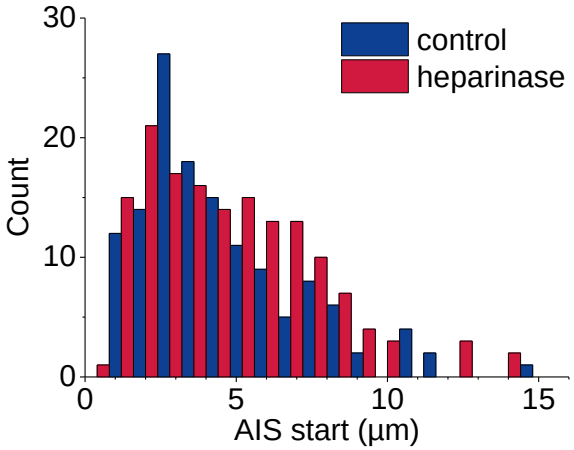

Distribution of axon initial segment start in control and heparinase-treated slices. The start of AnkG labelling (see figure 5 for an example) was considered the start of the axon initial segment (AIS). It was measured as the distance between the soma-hillock transition and the visually identified sharpest rise of AnkG labelling (experimenter blinded to treatment). Note the broad distribution of the AIS start (control 4.6 ± 0.26 µm, n = 135; heparinase 4.7 ± 0.23 µm, n = 154; *p* =0.74, unpaired t-test, coefficient of variation > 0.6 both groups).

References

Agronskaia AV, Tertoolen L & Gerritsen HC (2004). Fast fluorescence lifetime imaging of calcium in living cells. *J Biomed Opt* **9,** 1230–1237.

Dam GB ten, Hafmans T, Veerkamp JH & Kuppevelt TH van (2003). Differential Expression of Heparan Sulfate Domains in Rat Spleen. *J Histochem Cytochem* **51,** 727–739.

Ermolyuk YS, Alder FG, Henneberger C, Rusakov DA, Kullmann DM & Volynski KE (2012). Independent regulation of Basal neurotransmitter release efficacy by variable Ca^{2+} influx and bouton size at small central synapses. *PLoS Biol* **10,** e1001396.

Kochlamazashvili G, Henneberger C, Bukalo O, Dvoretskova E, Senkov O, Lievens PM-J, Westenbroek R, Engel AK, Catterall WA, Rusakov DA, Schachner M & Dityatev A (2010). The Extracellular Matrix Molecule Hyaluronic Acid Regulates Hippocampal Synaptic Plasticity by Modulating Postsynaptic L-Type Ca2+ Channels. *Neuron* **67,** 116–128.

Kurup S, Wijnhoven TJM, Jenniskens GJ, Kimata K, Habuchi H, Li J, Lindahl U, Kuppevelt TH van & Spillmann D (2007). Characterization of Anti-heparan Sulfate Phage Display Antibodies AO4B08 and HS4E4. *J Biol Chem* **282,** 21032–21042.

Zheng K, Bard L, Reynolds JP, King C, Jensen TP, Gourine AV & Rusakov DA (2015). Time-Resolved Imaging Reveals Heterogeneous Landscapes of Nanomolar Ca(2+) in Neurons and Astroglia. *Neuron* **88,** 277–288.